

Photoinduced Electrochemiluminescence Immunoassays

Dongni Han, Jasmina Vidic, Dechen Jiang,* Gabriel Loget,* and Neso Sojic*

Cite This: *Anal. Chem.* 2024, 96, 18262–18268

Read Online

ACCESS |



Metrics & More

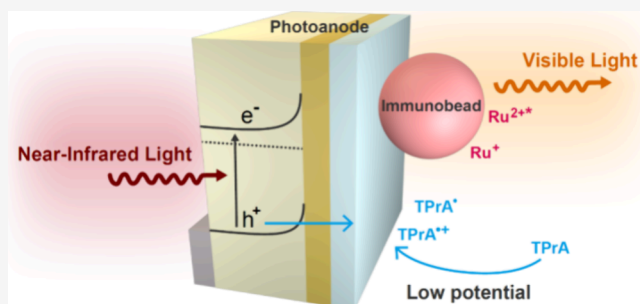


Article Recommendations



Supporting Information

ABSTRACT: Optimization of electrochemiluminescence (ECL) immunoassays is highly beneficial for enhancing clinical diagnostics. A major challenge is the improvement of the operation conditions required for the bead-based immunoassays using the typical $[\text{Ru}(\text{bpy})_3]^{2+}$ /tri-*n*-propylamine (TPrA) system. In this study, we report a heterogeneous immunoassay based on near-infrared photoinduced ECL, which facilitates the imaging and quantitative analysis of $[\text{Ru}(\text{bpy})_3]^{2+}$ -modified immunobeads at low anodic potential. The photovoltage generated by the photoanode under near-infrared light promotes oxidation processes at the electrode/electrolyte interface, thus considerably lowering the onset potential for both TPrA oxidation and ECL emission. The anti-Stokes shift between the excitation light (invisible to the human eyes) and the visible emitted light results in a clear and stable signal from the immunobeads. In addition, it offers the possibility of site-selective photoexcitation of the ECL process. This approach not only meets the performance of traditional ECL immunoassays in accuracy but also offers the additional benefits of lower potential requirements and enhanced stability, providing a new perspective for the optimization of commercial immunoassays.



INTRODUCTION

Immunoassay is one of the most powerful and sensitive technologies currently available for patient diagnosis and monitoring.¹ The basic principle involves labeling antigens or antibodies with markers, such as enzymes, radioisotopes, or luminophores, and indirectly determining the concentration of target molecules by detecting the signals from these labels.² Many immunoassays utilize magnetic beads as capture surfaces,^{3,4} employing them as solid-phase carriers to immobilize antigens or antibodies on their surfaces. This heterogeneous strategy allows for the separation, enrichment, and detection of targets through the application of an external magnetic field⁵ and thus offers several advantages. First, the three-dimensional structure of the beads increases the surface-to-volume ratio. Second, immobilizing biomolecules on the bead surface simplifies sample preprocessing. Additionally, different types of beads can provide a variety of functional surface characteristics, making it possible to conduct multiple detections simultaneously.

Electrochemiluminescence (ECL) is a technique that generates optical signals through electrochemical stimulation on the electrode surface.⁶ The most commonly used ECL systems include $[\text{Ru}(\text{bpy})_3]^{2+}$ and tri-*n*-propylamine (TPrA) as the luminophore and sacrificial co-reactant, respectively. In an ECL immunoassay (ECLIA), immunocomplexes captured by magnetic beads are labeled with a luminophore, typically a ruthenium chelate, which emits a detectable signal through reactions with TPrA radicals generated at the electrode interface.⁷ The electrochemical excitation characteristic of

ECL minimizes optical interference from the autofluorescence of the beads,⁸ resulting in extremely low detection limits.⁹ Since ECLIA is cost-effective and easily automated, over the past 30 years, it has been developed and successfully commercialized as a diagnostic and research tool.^{10–12} In clinical research, ECLIA is used to detect important biomolecules, including DNA, tumor markers, viruses, and hormones.^{13–16} In fundamental research, microscopy-based ECLIA has provided new insights into the ECL mechanism^{17–20} and has evolved to enable single biomolecule detection and multiplex immunoassays,^{21–23} establishing itself as a powerful microscopy technique.^{24–27}

Original approaches have been developed for generating stronger ECL signals.^{28–30} For example, ECL intensity was enhanced in both homogeneous and heterogeneous formats by emissive and non-emissive dual redox mediators.^{31–34} Zhu and co-workers boosted the ECL emission by inducing local heat through a laser procedure.³⁵ Another approach, named photoinduced ECL (PECL), is characterized by the combination of classical ECL systems with semiconductor photoelectrodes.^{29,36,37} This technique involves using specially designed semiconductor photoelectrodes, which absorb

Received: August 30, 2024

Revised: October 21, 2024

Accepted: October 24, 2024

Published: November 1, 2024



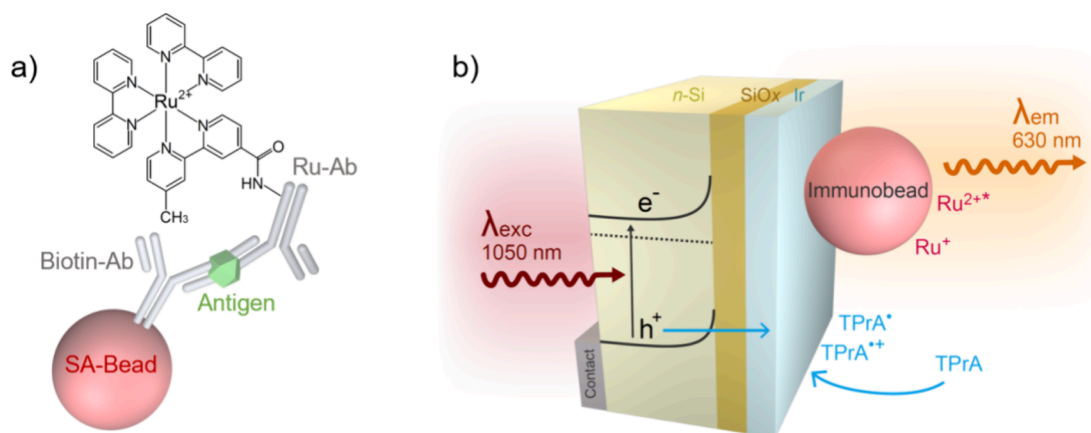


Figure 1. (a) Beads for EGFR detection with ECL readout. The immuno-sandwich complex consists of a capture antibody attached to 2.8 μm magnetic beads via biotin-streptavidin, the EGFR protein (antigen), and the ruthenylated detection antibody (denoted Ru-Ab). (b) Scheme of the PECL detection with back-illumination configuration. The $n\text{-Si/SiO}_x/\text{Ir}$ anode serves as the working electrode, excited by near-infrared light ($\lambda_{\text{exc}} = 1050 \text{ nm}$). PECL emission ($\lambda_{\text{em}} = 630 \text{ nm}$) of $[\text{Ru}(\text{bpy})_3]^{2+}$ labels attached to the beads is generated with the TPrA co-reactant in solution.

incident light at a given excitation wavelength (λ_{exc}), to generate photoinduced charge carriers. These carriers trigger the ECL reactions at the electrode/electrolyte interface, emitting light at a specific wavelength (λ_{em}) determined by the ECL luminophore. Due to the photovoltage generated at the photoelectrode, the excitation potential required for this special ECL is significantly reduced.^{38,39} This feature has enabled low-potential imaging of single cells and analysis of the catalytic activity of single nanocatalysts.^{40,41} Although early photoelectrodes used in PECL had poor stability, this problem has been addressed through the development of BiVO_4 photoanodes and metal–insulator–semiconductor (MIS) junction photoanodes.^{39,42,43} Remarkably, the $n\text{-Si/SiO}_x/\text{Ir}$ anode, as a kind of MIS photoanode, has demonstrated stable operation for over 35 h.³⁹ Therefore, this new ECL strategy holds promise for optimizing the performance of ECLIA.

Here, we introduce a low-potential bead-based immunoassay based on PECL using the $n\text{-Si/SiO}_x/\text{Ir}$ anode for epithelial growth factor receptor (EGFR) detection (Figure 1). EGFR was selected as the target analyte because it is an important indicator in the diagnosis and prognosis of various cancers.^{44,45} Benefiting from the photovoltage (approximately 300 mV) generated by the photoanode under near-infrared incident light ($\lambda_{\text{exc}} = 1050 \text{ nm}$), the onset potential of TPrA oxidation at the electrode interface is reduced, which subsequently lowers the onset potential of the ECL emission ($\lambda_{\text{em}} = 620 \text{ nm}$) from the immunobeads. This enables the photoelectrode to perform reliable immunoassays at an applied potential as low as 0.8 V (vs Ag/AgCl). Moreover, its anti-Stokes nature ($\lambda_{\text{exc}} > \lambda_{\text{em}}$) avoids the use of harmful incident light and ensures a high detection sensitivity. This low-potential immunoassay showcases its potential utility for developing a new class of ECL biosensors and can accelerate the optimization of commercial immunoassays.

EXPERIMENTAL SECTION

Reagents. Acetone (MOS electronic grade, Erbatron from Carlo Erba) and anhydrous ethanol (RSE electronic grade, Erbatron from Carlo Erba) were used without further purification. Sulfuric acid (96%) was acquired from BASF. Hydrogen peroxide (30%), bis(2,2'-bipyridine)-4'-methyl-4-carboxybipyridine-ruthenium *N*-succinimidyl ester-bis-(hexafluorophosphate) (ruthenium ester), and phosphate-

buffered saline (PBS) were obtained from Sigma-Aldrich. PBS (10 \times) was diluted with ultrapure Milli-Q water to create a 1 \times PBS solution. Streptavidin Dynabeads M-280 (streptavidin-coated magnetic beads with a diameter of 2.8 μm) and anhydrous dimethyl sulfoxide (DMSO) were provided by Invitrogen. Human EGFR antibody, recombinant human EGFR Fc chimera protein, and human EGFR biotinylated antibody were acquired from Bio-Techne. Bovine serum albumin blocking buffer (10% BSA) and dialysis cassettes (10K MWCO) were acquired from Thermo Scientific. The 0.1% BSA/PBS buffer was prepared using 10% BSA and 1 \times PBS. ProCell solution (containing 180 mM tripropylamine) was purchased from Roche.

Preparation of the Semiconductor Anode. All vials and tweezers used for cleaning silicon were previously decontaminated in 3/1 v/v concentrated $\text{H}_2\text{SO}_4/30\% \text{H}_2\text{O}_2$ at 105 $^\circ\text{C}$ for 30 min, followed by copious rinsing with ultrapure water. Caution: the concentrated aqueous $\text{H}_2\text{SO}_4/\text{H}_2\text{O}_2$ solution is very dangerous, particularly in contact with organic materials, and should be handled extremely carefully. The n -type silicon wafers (0.3–0.7 $\Omega \text{ cm}$ resistivity, phosphorus-doped, single side-polished, 475–525 μm) (100) and the p^{++} -type silicon wafers (0.001–0.005 $\Omega \text{ cm}$ resistivity, boron-doped, single side-polished, 490–510 μm) (100) were purchased from University Wafers. All the Si surfaces were degreased by sonication in acetone, ethanol, and ultrapure water for 10 min. The Si surfaces were then decontaminated and oxidized in piranha solution at 105 $^\circ\text{C}$ for 30 min, followed by rinsing with copious amounts of ultrapure water and dried under Ar flow. The 2 nm-thick Ir films were deposited on the clean p^{++} -Si/SiO $_x$ and n -Si/SiO $_x$ surfaces by sputtering with a Leica EM ACE600 coating system (Ir target purity: 99.95%, Neyco). The thickness of the film was controlled *in situ* using a quartz crystal microbalance. Then, the coated Si surfaces (1.3 \times 1.3 cm^2) were processed to fabricate the electrodes. An ohmic contact was done on the backside of the Si wafer by scratching the surface with a diamond glass cutter, and then a droplet of InGa eutectic (Sigma-Aldrich, 99.99%, metals basis) and a copper tape was applied on the scratched part. A thin layer of silver paste (Electron Microscopy Sciences) was painted to cover the InGa eutectic contact as well as a part of the copper tape. After the drying of the paste, Kapton tape was deposited to shield the backside for the protection of ohmic contact.³⁹

Immunobead Preparation. To synthesize the ruthenylated antibody, the ruthenium *N*-hydroxysuccinimidyl (NHS) ester luminophore reacted with the lysine residues of the antibody and formed a stable amide bond with it. Ruthenium NHS ester was diluted in DMSO to a concentration of 10 mg/mL and the EGFR antibody in 1× PBS to 0.2 mg/mL. These solutions were mixed at a volume ratio of 1:10 and left overnight at 4 °C. The mixture was dialyzed using 10K MWCO dialysis cassettes in 1× PBS for 2 h, and this step was repeated three times to remove unbound ruthenium. The final concentration of the ruthenylated antibody was approximately 20 μg/mL.

Then, the streptavidin-coated magnetic beads (10 mg/mL) were incubated with 0.2 mg/mL EGFR biotinylated antibody at a 1:1 volume ratio at 4 °C and mixed overnight. The beads were washed three times with 0.1% BSA/PBS buffer and twice with 1× PBS to eliminate unbound antibodies. Then, the antibody-coated beads were incubated with EGFR protein (0, 0.4, 2, 10, or 60 μg/mL, according to the needs) for 3 h at room temperature. The beads were washed three times with 1× PBS and then incubated with the ruthenylated antibody at a 1:10 volume ratio for 3 h at room temperature. Finally, the immuno-sandwich-modified beads were washed three times with 0.1% BSA/PBS buffer and twice with 1× PBS before use.

Device for Imaging. The PECL cell was a 3-electrode system adapted on a P-type chamber from Idylle (www.idylle-labs.com) with a working electrode (*n*-Si/SiO_x/Ir or *p*⁺-Si/SiO_x/Ir), a platinum wire (Pt) as the counter electrode, and 3 M Ag/AgCl/KCl electrode as the reference electrode. The ECL cell for experiments with a glassy carbon electrode was a 3-electrode system adapted on a C-type chamber from Idylle with the same counter electrode and reference electrode as the PECL cell. The experiments were performed using a PalmSens4 potentiostat, while the surface was illuminated on the backside (on the *n*-Si side) by an LED at 1050 nm (Thorlabs, M1050L4). The fluorescence and PECL images were recorded on the front side (the Ir side) of the surface using an epifluorescence inverted microscope (Leica DM18) and an electron-multiplying charge-coupled device (EM-CCD 9100-13) camera from Hamamatsu (see Figure S1).

A 40× objective (Leica HC APO; water immersion) with a 0.8 numerical aperture was used for the PECL and fluorescence experiments. The ECL imaging was performed as a control experiment in the same conditions but using a *p*⁺-Si/SiO_x/Ir surface or a glassy carbon electrode as the working electrode and without the need of illumination by the infrared LED. The images were treated and analyzed by ImageJ-Fiji software (open source).

PECL and ECL Imaging. The PL images of the beads labeled with [Ru(bpy)₃]²⁺ were captured using a normal CCD and a long-pass FITC filter ($\lambda_{\text{exc}} = 470 \pm 20$ nm; $\lambda_{\text{DM}} = 510$ nm; $\lambda_{\text{Suppr}} = \text{LP } 515$ nm) with an exposure time of 0.2 s. The PECL and ECL images were captured with an EMCCD (sensitivity gain = 255; gain = 1) using a short-pass IR filter (cutoff of 750 nm) and an exposure time of 5 s. The intensity curves of the beads in Figure 2b were measured from a set of PECL/ECL images recorded simultaneously with cyclic voltammetry, with each image having an exposure time of 1 s.

RESULTS AND DISCUSSION

Manufacturing of the Near-Infrared PECL System.

Silicon (Si) is an inorganic semiconductor material with a narrow bandgap of 1.12 eV (corresponding to 1110 nm),

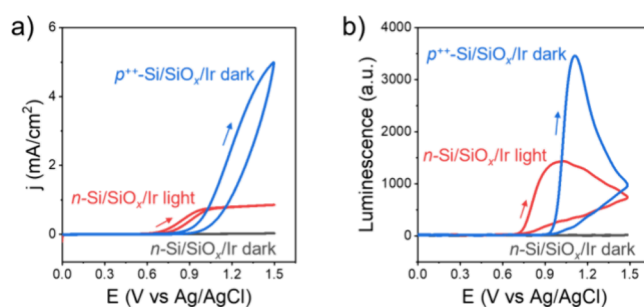


Figure 2. (a) Current density and (b) corresponding ECL signals of the *n*-Si/SiO_x/Ir anode in the dark (gray curve) or under 1050 nm infrared illumination (red curve) and the *p*⁺-Si/SiO_x/Ir anode in the dark (blue curve) during cyclic voltammetry in ProCell solution (containing 180 mM TPrA). Both anodes were modified with EGFR immunobeads at a concentration of 10 μg/mL. Scan rate: 50 mV/s.

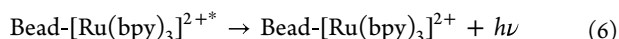
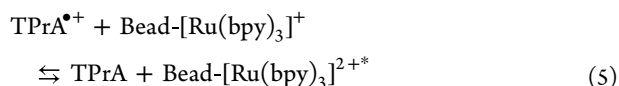
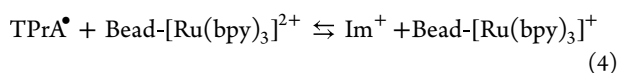
making it ideal for absorbing near-infrared excitation light.^{46,47} This property enables the separation of the visible light emission of ECL luminophores, such as ruthenium chelates and luminol, from the excitation light of Si-based photoelectrodes.⁴⁸ Also, the excellent surface chemical properties and processability of Si make it a reliable working electrode in biosensing.⁴⁹ However, Si-based photoelectrodes can undergo passivation and photocorrosion in the aqueous electrolytes required for immunoassays.^{50–52} To overcome these issues, the *n*-Si/SiO_x/Ir photoanode with a MIS junction was used in this study.^{39,53} In this configuration, *n*-type Si (moderately doped with phosphorus) serves as the absorber component of the photoanode, responding to irradiation and generating photoinduced charge carriers. The 1.5 nm-thick SiO_x layer is expected to improve photovoltage while enabling charge tunneling.⁵⁴ The 2 nm-thick Ir layer ensures charge collection, protects Si from passivation, and catalyzes the ECL reaction.³⁹ Its anticorrosion property and high catalytic activity make it suitable for long-term electrochemical processes.⁵⁵ Given these advantages, the *n*-Si/SiO_x/Ir anode was employed in PECL immunoassays.

The model ECL system, [Ru(bpy)₃]²⁺ and TPrA, was chosen as the luminophore and co-reactant, respectively. To allow EGFR recognition, the ruthenylated EGFR antibodies were immobilized on 2.8 μm magnetic beads through an immuno-sandwich structure (Figure 1a), where the amount of [Ru(bpy)₃]²⁺ labels bound to each bead surface reflects the concentration of the EGFR protein. The reaction cell contained ProCell solution with 180 mM TPrA, along with a Pt counter electrode, an Ag/AgCl (3 M KCl) reference electrode, and the *n*-Si/SiO_x/Ir anode coated with beads. Near-infrared light at 1050 nm was used as the incident light (Figure 1b). Its photon energy exceeds the bandgap energy of Si, which generates photoinduced electron–hole pairs within the photoanode. The built-in electric field drives holes toward the Ir layer, creating a potential difference (i.e., photovoltage) in the depletion region that facilitates TPrA oxidation at the electrode/electrolyte interface.³⁷ At the interface, the photovoltage and applied potential induce together the TPrA oxidation, forming TPrA radical cations that deprotonate to neutral TPrA radicals. These radicals react with [Ru(bpy)₃]²⁺ decorating the beads and generating the excited state of the labels.^{17,56} As the excited state returns to the ground state, it emits photons at 630 nm. The significant wavelength difference between excitation (1050 nm) and emission (630

nm) wavelengths allows for the use of a 750 nm short-pass filter to isolate pure emission light (Figure S1), whose intensity serves as a quantitative indicator for the immunoassay.

Notably, backside illumination was employed to separate the location of light absorption from the surface reaction site and to minimize the decomposition of the photosensitive $[\text{Ru}(\text{bpy})_3]^{2+}$.^{57–59} The penetration of the excitation light into Si ensures an abundance of photoinduced carriers on the front side of the photoanode.⁶⁰

Low-Potential Immunobead Imaging. To study the near-infrared PECL immunoassays, we examined the photoelectrochemical response of a photoactive $n\text{-Si}/\text{SiO}_x/\text{Ir}$ anode under near-infrared (1050 nm) illumination and the corresponding ECL behavior. The photoanode, loaded with $[\text{Ru}(\text{bpy})_3]^{2+}$ -modified immunobeads, was immersed in ProCell solution, and their electrochemical and ECL properties were investigated first by cyclic voltammetry. As shown in Figure 2a,b, both the current density and luminescence were nearly zero under dark conditions, indicating a lack of charge flow and electrochemical inactivity. This phenomenon can be attributed to the inhibition of oxidation reactions at the interface by the rectifying nature of the MIS junction.⁶¹ However, when illuminated at 1050 nm, a noticeable photocurrent was observed starting at 0.6 V, indicating the onset of TPrA oxidation at the anode interface. This value is lower than the onset oxidation potential of TPrA on conventional working electrodes (Figure S2). The light signal from the beads appeared at 0.7 V, suggesting that the TPrA \cdot neutral radicals and TPrA \cdot^+ radical cations at the anode interface were sufficient to effectively induce the formation of the excited state of $[\text{Ru}(\text{bpy})_3]^{2+}$ under these experimental conditions. TPrA oxidation and the reactivity of the TPrA radical govern the ECL process.^{17,18,56,62} The heterogeneous immunoassay follows the mechanism:



where Im^+ is the iminium product, and $\text{Bead-}[\text{Ru}(\text{bpy})_3]^{2+}$ represents an immunobead with the bound ECL labels.

To evaluate whether the light signal of beads benefits from the photovoltage and photocurrent generated by the photoanode, a nonphotoactive highly doped $p^{++}\text{-Si}/\text{SiO}_x/\text{Ir}$ anode (highly doped with boron) was tested for comparison. Under dark conditions, the oxidation current of TPrA with the $p^{++}\text{-Si}/\text{SiO}_x/\text{Ir}$ anode began to appear at 0.8 V (Figure 2a), and the ECL signal from the beads was captured by the EMCCD starting at 1 V (Figure 2b). In the dark, TPrA oxidation on the $p^{++}\text{-Si}/\text{SiO}_x/\text{Ir}$ anode surface only relies on the applied potential since it is not limited by the density of holes in the p^{++} -type Si. Consequently, the onset potentials for co-reactant oxidation and the ECL signal of the $p^{++}\text{-Si}/\text{SiO}_x/\text{Ir}$ anode are significantly shifted compared to those with the $n\text{-Si}/\text{SiO}_x/\text{Ir}$

anode. The measured 300 mV shift in the ECL onset potential reflects the photovoltage of the photoanode; this value is consistent with previously reported results.^{38–40}

It should be noted that the oxidation current density of the $p^{++}\text{-Si}/\text{SiO}_x/\text{Ir}$ anode increases with the applied potential, while the photocurrent density of the $n\text{-Si}/\text{SiO}_x/\text{Ir}$ anode saturates beyond a certain potential due to the limitation in absorbed photons. This characteristic also confirms that the electrochemical processes and the generation of the PECL signal on the $n\text{-Si}/\text{SiO}_x/\text{Ir}$ anode are facilitated by the photoinduced carriers at the electrode/electrolyte interface.

Based on the observation that the PECL onset potential is lower than the ECL onset potential, we optimized the excitation conditions for PECL in immunoassays. While a voltage of 0.7 V allows the EMCCD to capture the PECL signal from the immunobeads, the signal intensity falls short of meeting the demand for highly sensitive immunoassays. To balance applying the lowest possible external potential with achieving high-quality imaging, we determined that 0.8 V is a more appropriate voltage (Figure S3).

In traditional ECLIA, glassy carbon is considered one of the best electrode materials.^{17,22} Therefore, we compared the performance of the $n\text{-Si}/\text{SiO}_x/\text{Ir}$ anode, the $p^{++}\text{-Si}/\text{SiO}_x/\text{Ir}$ anode, and the glassy carbon electrode for imaging beads under the potential of 0.8 V. As shown in Figure 3a, the

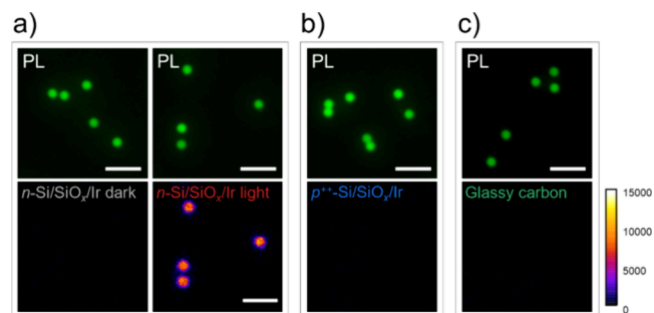


Figure 3. PL and ECL images of $[\text{Ru}(\text{bpy})_3]^{2+}$ -modified immunobeads (diameter of 2.8 μm , 10 $\mu\text{g}/\text{mL}$ EGFR) recorded in ProCell solution containing 180 mM TPrA at 0.8 V (a) on an $n\text{-Si}/\text{SiO}_x/\text{Ir}$ anode (without and with infrared illumination), (b) on a $p^{++}\text{-Si}/\text{SiO}_x/\text{Ir}$ anode, and (c) on a glassy carbon electrode. Exposure time of the EMCCD camera: 5 s. Scale bars: 10 μm .

photoactive $n\text{-Si}/\text{SiO}_x/\text{Ir}$ anode produced bead PECL signals only when effective excitation illumination and sufficient external potential were provided. In contrast, neither the nonphotoactive $p^{++}\text{-Si}/\text{SiO}_x/\text{Ir}$ anode nor the glassy carbon electrode generated any visible ECL signal from the beads at the same potential (Figure 3b,c). The bead ECL signal was only observed when a higher potential was imposed (Figure S4). These results indicate that the $n\text{-Si}/\text{SiO}_x/\text{Ir}$ anode was superior compared to other working electrodes for immunoassays, capable of operating at low onset anodic potentials. This characteristic provides it with important potential for use in immunoanalytical applications.

PECL Immunoassay. The $n\text{-Si}/\text{SiO}_x/\text{Ir}$ anode was then utilized for PECL immunoassays to evaluate its practical performance. In this approach, capture antibodies, EGFR proteins, and ruthenylated detection antibodies were sequentially attached to magnetic beads using a sandwich method (Figure 1). The PECL intensity of the beads is directly proportional to the EGFR concentration in the sandwich. As

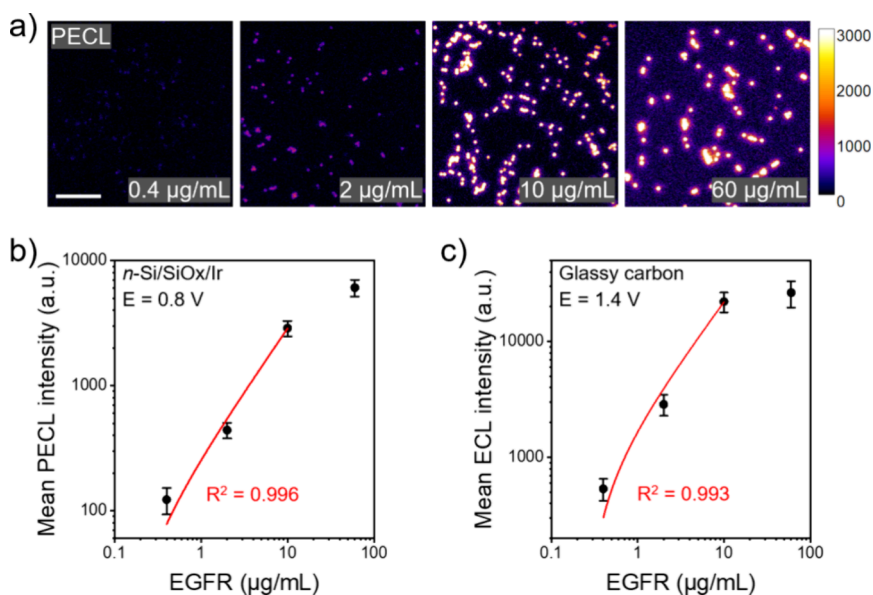


Figure 4. (a) PECL images of immunobeads with varying EGFR concentrations (0.4–60 µg/mL) under infrared illumination at 0.8 V on *n*-Si/SiO_x/Ir anodes in ProCell solution. Exposure time: 5 s. Scale bar: 50 µm. (b) Mean PECL intensity of single beads at various EGFR concentrations measured from PECL images in panel (a). *n* = 48, 20, 84, and 44. (c) Mean ECL intensity of single beads at various EGFR concentrations measured from ECL images recorded on glassy carbon electrodes at 1.4 V in ProCell solution containing 180 mM TPrA. *n* = 18, 61, 28, and 47.

shown in Figure 4a, the light signal of the beads increased with rising concentrations of EGFR. Measurements revealed a strong linear relationship between PECL intensity and EGFR concentration below 10 µg/mL (Figure 4b). At higher concentrations, this linearity decreased due to the saturation of antibody binding sites.⁶³

As a control, bead-based ECLIA was also conducted using glassy carbon electrodes (Figure S5). The results were similar to those obtained with the photoanode-based PECL (Figure 4c), confirming the accuracy and stability of the PECL immunoassay. Notably, the ECLIA using glassy carbon electrodes required a potential of 1.4 V, a value commonly used in many studies.^{18,64} In contrast, the *n*-Si/SiO_x/Ir anode achieved the same performance at only 0.8 V under near-infrared illumination, making this low-voltage detection method commercially appealing.

Moreover, the surface properties and oxidation current density on the glassy carbon electrode often degrade during the ECL process with repeated use, which affects its lifespan in practical operations.¹⁹ Fortunately, the *n*-Si/SiO_x/Ir anode did not encounter this issue; even after multiple excitations, the current density remained consistent (Figure S6), ensuring stable electrochemical processes at the electrode interface. Therefore, the near-infrared PECL immunoassay based on the *n*-Si/SiO_x/Ir photoanode is both reliable and robust. Additionally, the light-induced excitation process of PECL enables site-selective detection for multiplex immunoassays on a single photoanode, representing a promising multiplex approach.

CONCLUSIONS

In this study, we present a bead-based PECL immunoassay. Using a MIS *n*-Si/SiO_x/Ir photoanode and near-infrared incident light, low-potential imaging of immunobeads was successfully achieved. The anti-Stokes shift between the invisible excitation light and the visible emission ensures a clear and stable PECL signal. The photoanode generates a photovoltage of nearly 300 mV under illumination, enabling

high-quality imaging at a potential as low as 0.8 V. The PECL immunoassay performs as well as traditional ECL immunoassays while offering the added benefits of low potential and high stability. At the end, this approach provides a novel format for ECL immunoassays and offers new insights for optimizing successfully commercialized immunoassays.

ASSOCIATED CONTENT

Supporting Information

The Supporting Information is available free of charge at <https://pubs.acs.org/doi/10.1021/acs.analchem.4c04662>.

Schematic of the setup; more PECL and ECL images; chronoamperometric curves (PDF)

AUTHOR INFORMATION

Corresponding Authors

Dechen Jiang – State Key Laboratory of Analytical Chemistry for Life Science and School of Chemistry and Chemical Engineering, Nanjing University, Nanjing, Jiangsu 210093, China; orcid.org/0000-0002-2845-3621; Email: dechenjiang@nju.edu.cn

Gabriel Loget – Univ. Bordeaux, Bordeaux INP, CNRS, UMR 5255, ENSMAC, Pessac 33607, France; orcid.org/0000-0003-4809-5013; Email: gabriel.loget@cnrs.fr

Neso Sojic – Univ. Bordeaux, Bordeaux INP, CNRS, UMR 5255, ENSMAC, Pessac 33607, France; orcid.org/0000-0001-5144-1015; Email: sojic@u-bordeaux.fr

Authors

Dongni Han – Univ. Bordeaux, Bordeaux INP, CNRS, UMR 5255, ENSMAC, Pessac 33607, France; State Key Laboratory of Analytical Chemistry for Life Science and School of Chemistry and Chemical Engineering, Nanjing University, Nanjing, Jiangsu 210093, China

Jasmina Vidic – INRAE, AgroParisTech, Micalis Institute, UMR 1319, Université Paris-Saclay, Jouy-en-Josas 78350, France; orcid.org/0000-0002-8549-8199

Complete contact information is available at:
<https://pubs.acs.org/10.1021/acs.analchem.4c04662>

Notes

The authors declare no competing financial interest.

ACKNOWLEDGMENTS

This work is kindly supported by the Agence Nationale de la Recherche (ELISE-ANR-21-CE42), the Sino-French International Research Network ELECTROSENS (CNRS), and the Chinese Scholarship Council. The authors gratefully acknowledge the financial support of the European Union (grant agreement no. 101135402, Mobiles project).

REFERENCES

- (1) Cox, K. L.; Devanarayan, V.; Kriauciunas, A.; Manetta, J.; Montrose, C.; Sittampalam, S. *Immunoassay Methods*. In *Assay Guidance Manual*; 2019.
- (2) Pei, X.; Zhang, B.; Tang, J.; Liu, B.; Lai, W.; Tang, D. *Anal. Chim. Acta* **2013**, *758*, 1–18.
- (3) Yang, S.-Y.; Lien, K.-Y.; Huang, K.-J.; Lei, H.-Y.; Lee, G.-B. *Biosens. Bioelectron.* **2008**, *24* (4), 855–862.
- (4) Huergo, L. F.; Selim, K. A.; Conzentino, M. S.; Gerhardt, E. C. M.; Santos, A. R. S.; Wagner, B.; Alford, J. T.; Deobald, N.; Pedrosa, F. O.; de Souza, E. M.; Nogueira, M. B.; Raboni, S. M.; Souto, D.; Rego, F. G. M.; Zquette, D. L.; Aoki, M. N.; Nardin, J. M.; Fornazari, B.; Morales, H. M. P.; Borges, V. A.; Nelde, A.; Walz, J. S.; Becker, M.; Schneiderhan-Marra, N.; Rothbauer, U.; Reis, R. A.; Forchhammer, K. *ACS Sens.* **2021**, *6* (3), 703–708.
- (5) Gijs, M. A.; Lacharme, F.; Lehmann, U. *Chem. Rev.* **2010**, *110* (3), 1518–1563.
- (6) Sojic, N. *Analytical Electrogenenerated Chemiluminescence: From Fundamentals to Bioassays*; Royal Society of Chemistry: 2019.
- (7) Giagu, G.; Fracassa, A.; Fiorani, A.; Villani, E.; Paolucci, F.; Valenti, G.; Zanut, A. *Microchim. Acta* **2024**, *191* (6), 359.
- (8) Roth, S.; Hadass, O.; Cohen, M.; Verbarq, J.; Wilsey, J.; Danielli, A. *Small* **2019**, *15* (3), No. 1803751.
- (9) Wang, Y.; Ding, J.; Zhou, P.; Liu, J.; Qiao, Z.; Yu, K.; Jiang, J.; Su, B. *Angew. Chem., Int. Ed.* **2023**, *62* (16), No. e202216525.
- (10) Muzyka, K. *Biosens. Bioelectron.* **2014**, *54*, 393–407.
- (11) Lippi, G.; Henry, B. M.; Adeli, K. *Clin. Chem. Lab. Med.* **2022**, *60* (5), 655–661.
- (12) Parai, D.; Dash, G. C.; Choudhary, H. R.; Peter, A.; Rout, U. K.; Nanda, R. R.; Kshatri, J. S.; Kanungo, S.; Pati, S.; Bhattacharya, D. *J. Virol. Methods* **2021**, *292*, No. 114121.
- (13) Zhang, H.-R.; Xu, J.-J.; Chen, H.-Y. *Anal. Chem.* **2013**, *85* (11), 5321–5325.
- (14) Chen, Y.; Ye, Z.; Ma, M.; Yang, J.; Liu, R.; Zhang, Y.; Ma, P.; Song, D. *Biosens. Bioelectron.* **2024**, *254*, No. 116241.
- (15) Nikolaou, P.; Sciuto, E. L.; Zanut, A.; Petralia, S.; Valenti, G.; Paolucci, F.; Prodi, L.; Conoci, S. *Biosens. Bioelectron.* **2022**, *209*, No. 114165.
- (16) Kuang, K.; Chen, Y.; Li, Y.; Ji, Y.; Jia, N. *Biosens. Bioelectron.* **2024**, *247*, No. 115914.
- (17) Sentic, M.; Milutinovic, M.; Kanoufi, F.; Manojlovic, D.; Arbault, S.; Sojic, N. *Chem. Sci.* **2014**, *5* (6), 2568–2572.
- (18) Zanut, A.; Fiorani, A.; Canola, S.; Saito, T.; Ziebart, N.; Rapino, S.; Rebecani, S.; Barbon, A.; Irie, T.; Josel, H. P.; Negri, F.; Marcaccio, M.; Windfuhr, M.; Imai, K.; Valenti, G.; Paolucci, F. *Nat. Commun.* **2020**, *11* (1), 2668.
- (19) Dutta, P.; Han, D.; Goudeau, B.; Jiang, D.; Fang, D.; Sojic, N. *Biosens. Bioelectron.* **2020**, *165*, No. 112372.
- (20) Han, D.; Jiang, D.; Valenti, G.; Paolucci, F.; Kanoufi, F.; Chaumet, P. C.; Fang, D.; Sojic, N. *ACS Sens.* **2023**, *8* (12), 4782–4791.
- (21) Zhu, W.; Dong, J.; Ruan, G.; Zhou, Y.; Feng, J. *Angew. Chem., Int. Ed.* **2023**, *62* (7), No. e202214419.
- (22) Yang, X.; Hang, J.; Qu, W.; Wang, Y.; Wang, L.; Zhou, P.; Ding, H.; Su, B.; Lei, J.; Guo, W.; et al. *J. Am. Chem. Soc.* **2023**, *145* (29), 16026–16036.
- (23) Deiss, F.; LaFratta, C. N.; Symer, M.; Blicharz, T. M.; Sojic, N.; Walt, D. R. *J. Am. Chem. Soc.* **2009**, *131* (17), 6088–6089.
- (24) Zanut, A.; Fiorani, A.; Rebecani, S.; Kesarkar, S.; Valenti, G. *Anal. Bioanal. Chem.* **2019**, *411*, 4375–4382.
- (25) Rebecani, S.; Zanut, A.; Santo, C. I.; Valenti, G.; Paolucci, F. *Anal. Chem.* **2022**, *94* (1), 336–348.
- (26) Ma, C.; Cao, Y.; Gou, X.; Zhu, J.-J. *Anal. Chem.* **2020**, *92* (1), 431–454.
- (27) Qi, H.; Zhang, C. *Anal. Chem.* **2020**, *92* (1), 524–534.
- (28) Li, H.; Bouffier, L.; Arbault, S.; Kuhn, A.; Hogan, C. F.; Sojic, N. *Electrochem. Commun.* **2017**, *77*, 10–13.
- (29) Zhao, Y.; Bouffier, L.; Xu, G.; Loget, G.; Sojic, N. *Chem. Sci.* **2022**, *13* (9), 2528–2550.
- (30) Zhao, Y.; Descamps, J.; AlHoda Al Bast, N.; Duque, M.; Esteve, J.; Sepulveda, B.; Loget, G.; Sojic, N. *J. Am. Chem. Soc.* **2023**, *145* (31), 17420–17426.
- (31) Kerr, E.; Hayne, D. J.; Soulsby, L. C.; Bawden, J. C.; Blom, S. J.; Doeven, E. H.; Henderson, L. C.; Hogan, C. F.; Francis, P. S. *Chem. Sci.* **2022**, *13* (2), 469–477.
- (32) Kerr, E.; Knezevic, S.; Francis, P. S.; Hogan, C. F.; Valenti, G.; Paolucci, F.; Kanoufi, F.; Sojic, N. *ACS Sens.* **2023**, *8* (2), 933–939.
- (33) Fracassa, A.; Santo, C. I.; Kerr, E.; Knežević, S.; Hayne, D. J.; Francis, P. S.; Kanoufi, F.; Sojic, N.; Paolucci, F.; Valenti, G. *Chem. Sci.* **2024**, *15* (3), 1150–1158.
- (34) Adamson, N. S.; Blom, S. J.; Doeven, E. H.; Connell, T. U.; Hadden, C.; Knežević, S.; Sojic, N.; Fracassa, A.; Valenti, G.; Paolucci, F.; et al. *Angew. Chem., Int. Ed.* **2024**.
- (35) Gou, X.; Zhang, Y.; Xing, Z.; Ma, C.; Mao, C.; Zhu, J. J. *Chem. Sci.* **2023**, *14* (34), 9074–9085.
- (36) Zhao, Y.; Descamps, J.; Léger, Y.; Sojic, N.; Loget, G. *Acc. Chem. Res.* **2024**, *57* (15), 2144–2153.
- (37) Vogel, Y. B.; Gooding, J. J.; Ciampi, S. *Chem. Soc. Rev.* **2019**, *48* (14), 3723–3739.
- (38) Zhao, Y.; Yu, J.; Xu, G.; Sojic, N.; Loget, G. *J. Am. Chem. Soc.* **2019**, *141* (33), 13013–13016.
- (39) Zhao, Y.; Descamps, J.; Ababou-Girard, S.; Bergamini, J. F.; Santinacci, L.; Leger, Y.; Sojic, N.; Loget, G. *Angew. Chem., Int. Ed.* **2022**, *61* (20), No. e202201865.
- (40) Descamps, J.; Zhao, Y.; Goudeau, B.; Manojlovic, D.; Loget, G.; Sojic, N. *Chem. Sci.* **2024**, *15* (6), 2055–2061.
- (41) Xue, J. W.; Xu, C. H.; Zhao, W.; Chen, H. Y.; Xu, J. J. *Nano Lett.* **2023**, *23* (10), 4572–4578.
- (42) Yu, J.; Saada, H.; Abdallah, R.; Loget, G.; Sojic, N. *Angew. Chem., Int. Ed.* **2020**, *59* (35), 15157–15160.
- (43) Descamps, J.; Zhao, Y.; Le-Pouliquen, J.; Goudeau, B.; Garrigue, P.; Tavernier, K.; Léger, Y.; Loget, G.; Sojic, N. *Chem. Commun.* **2023**, *59* (82), 12262–12265.
- (44) Nicholson, R. I.; Gee, J. M. W.; Harper, M. E. *Eur. J. Cancer* **2001**, *37*, 9–15.
- (45) Tol, J.; Dijkstra, J. R.; Klomp, M.; Teerenstra, S.; Dommerholt, M.; Vink-Börger, M. E.; van Cleef, P. H.; van Krieken, J. H.; Punt, C. J. A.; Nagtegaal, I. D. *Eur. J. Cancer* **2010**, *46* (11), 1997–2009.
- (46) Shur, M. S. *Handbook Series on Semiconductor Parameters*; World Scientific: 1996.
- (47) Dabboussi, J.; Zhao, Y.; Abdallah, R.; Gicquel, A.; Bendavid, C.; Loget, G. *Biosens. Bioelectron.: X* **2022**, *12*, No. 100221.
- (48) Abdussalam, A.; Xu, G. *Anal. Bioanal. Chem.* **2022**, *414* (1), 131–146.
- (49) Yakovleva, J.; Davidsson, R.; Lobanova, A.; Bengtsson, M.; Eremin, S.; Laurell, T.; Emnéus, J. *Anal. Chem.* **2002**, *74* (13), 2994–3004.
- (50) Bae, D.; Seger, B.; Vesborg, P. C.; Hansen, O.; Chorkendorff, I. *Chem. Soc. Rev.* **2017**, *46* (7), 1933–1954.
- (51) Zhang, X. G. *Electrochemistry of Silicon and Its Oxide*; Springer Science & Business Media: 2001.
- (52) Fabre, B.; Loget, G. *Acc. Mater. Res.* **2023**, *4* (2), 133–142.

- (53) Sibü, G. A.; Gayathri, P.; Akila, T.; Marnadu, R.; Balasubramani, V. *Nano Energy* **2024**, *125*, No. 109534.
- (54) Sun, K.; Shen, S.; Liang, Y.; Burrows, P. E.; Mao, S. S.; Wang, D. *Chem. Rev.* **2014**, *114* (17), 8662–8719.
- (55) Chen, Z.; Duan, X.; Wei, W.; Wang, S.; Ni, B.-J. *Nano Energy* **2020**, *78*, No. 105270.
- (56) Miao, W.; Choi, J. P.; Bard, A. J. *J. Am. Chem. Soc.* **2002**, *124* (48), 14478–14485.
- (57) Liu, B.; Wang, T.; Wang, S.; Zhang, G.; Zhong, D.; Yuan, T.; Dong, H.; Wu, B.; Gong, J. *Nat. Commun.* **2022**, *13* (1), 7111.
- (58) Fuller, Z. J.; Bare, W. D.; Kneas, K. A.; Xu, W. Y.; Demas, J. N.; DeGraff, B. A. *Anal. Chem.* **2003**, *75* (11), 2670–2677.
- (59) Han, D.; Goudeau, B.; Manojlovic, D.; Jiang, D.; Fang, D.; Sojic, N. *Angew. Chem., Int. Ed.* **2021**, *60* (14), 7686–7690.
- (60) Saritaş, M.; McKell, H. D. *J. Appl. Phys.* **1987**, *61* (10), 4923–4925.
- (61) Memming, R. *Semiconductor Electrochemistry*; John Wiley & Sons: 2015.
- (62) Mariani, C.; Bogialli, S.; Paolucci, F.; Pastore, P.; Zanut, A.; Valenti, G. *Electrochim. Acta* **2024**, *489*, No. 144256.
- (63) Porstmann, T.; Kiessig, S. T. *J. Immunol. Methods* **1992**, *150* (1–2), 5–21.
- (64) Fiorani, A.; Han, D.; Jiang, D.; Fang, D.; Paolucci, F.; Sojic, N.; Valenti, G. *Chem. Sci.* **2020**, *11* (38), 10496–10500.